Perfusion imaging heterogeneity during NO inhalation distinguishes pulmonary arterial hypertension (PAH) from healthy subjects and has potential as an imaging biomarker

Tilo Winkler PhD[1], Puja Kohli MD MMSc[2], Vanessa J Kelly PhD[2], Ekaterina G. Kehl MD[2], Alison S. Witkin, MD[2], Josanna Rodriguez-Lopez MD[2], Kathryn A. Hibbert MD[2], Mamary Kone MD MPH[2], David M. Systrom MD[3], Aaron B. Waxman MD[3], Jose G. Venegas PhD[1], Richard Channick MD[2], R. Scott Harris MD[2]

[1] Department of Anesthesia, Critical Care and Pain Medicine, Massachusetts General Hospital and Harvard Medical School, Boston, Massachusetts
[2] Division of Pulmonary and Critical Care Medicine, Department of Medicine, Massachusetts General Hospital and Harvard Medical School, Boston, Massachusetts
[3] Division of Pulmonary and Critical Care Medicine, Department of Medicine, Brigham and Women's Hospital and Harvard Medical School, Boston, Massachusetts

ORCID

Tilo Winkler	https://orcid.org/0000-0002-7276-5550
Kathryn A. Hibbert	https://orcid.org/0000-0001-7908-5446
David M. Systrom	https://orcid.org/0000-0002-9610-6330
Aaron B. Waxman	https://orcid.org/0000-0001-7797-0361

Corresponding author:
Tilo Winkler, PhD
Massachusetts General Hospital
Dept of Anesthesia, Critical Care and Pain Medicine
55 Fruit Street, Boston, MA 02114
USA
Email address: twinkler@mgh.harvard.edu
Phone: ++1-617-724-4083

ABSTRACT

Background: Without aggressive treatment, pulmonary arterial hypertension (PAH) has a 5-year mortality of approximately 40%. A patient's response to vasodilators at diagnosis impacts the therapeutic options and prognosis. We hypothesized that analyzing perfusion images acquired before and during vasodilation could identify characteristic differences between PAH and control subjects.

Methods: We studied 5 controls and 4 subjects with PAH using HRCT and ^{13}NN PET imaging of pulmonary perfusion and ventilation. The total spatial heterogeneity of perfusion (CV^2_{Qtotal}) and its components in the vertical (CV^2_{Qvgrad}) and cranio-caudal (CV^2_{Qzgrad}) directions, and the residual heterogeneity (CV^2_{Qr}), were assessed at baseline and while breathing oxygen and nitric oxide (O_2+iNO). The length scale spectrum of CV^2_{Qr} was determined from 10 to 110 mm, and the response of regional perfusion to O_2+iNO was calculated as the mean of absolute differences. Vertical gradients in perfusion (Q_{vgrad}) were derived from perfusion images, and ventilation-perfusion distributions from images of ^{13}NN washout kinetics.

Results: O_2+iNO significantly enhanced perfusion distribution differences between PAH and controls, allowing differentiation between PAH subjects from controls. During O_2+iNO, CV^2_{Qvgrad} was significantly higher in controls than in PAH (0.08 (0.055-0.10) vs. 6.7 x 10^{-3} (2x10^{-4}-0.02), $p<0.001$) with a considerable gap between groups. Q_{vgrad} and CV^2_{Qtotal} showed smaller differences: –7.3 vs. -2.5, $p = 0.002$, and 0.12 vs. 0.06, $p = 0.01$. CV^2_{Qvgrad} had the largest effect size among the primary parameters during O_2+iNO. CV^2_{Qr}, and its length scale spectrum were similar in PAH and controls. Ventilation-perfusion distributions showed a trend towards a difference between PAH and controls at baseline, but it was not statistically significant.

Conclusions: Perfusion imaging during O2+iNO showed a significant difference in the heterogeneity associated with the vertical gradient in perfusion, distinguishing PAH subjects from controls.

Trial registration: Not applicable

KEYWORDS

Pulmonary Circulation

Vascular Physiology

Functional Imaging

Positron Emission Tomography

Perfusion distribution

Ventilation/Perfusion distribution

Inhaled nitric oxide

INTRODUCTION

Pulmonary arterial hypertension (PAH) is a progressive disease with a 5-year mortality, if not aggressively treated, of approximately 40% [1]. Wide variations in patients' response to vasodilator treatment is a major challenge to improving outcomes [2]. Treatment guidelines define a positive response to the vasodilator challenge as a reduction of the mean pulmonary arterial pressure (mPAP) ≥ 10 mmHg to reach an absolute value of mPAP ≤ 40 mmHg with an increased or unchanged cardiac output [3]. But, only about 10% of patients with idiopathic PAH meet these clinical criteria for a response to vasodilators [3] that allow greater treatment options and have better survival [2,3]. Interestingly, it has been shown that the magnitude of responses in pulmonary vascular resistance (PVR) or mean PAP to inhaled nitric oxide with oxygen predicts long-term survival even among patient that are non-responders [4]. Overall, however, we have little insight to date into the pulmonary vascular function that is associated with increased risk.

In contrast to global parameters such as mPAP or pulmonary vascular resistance (PVR), imaging of pulmonary perfusion provides insights into regional changes associated with the disease process and its heterogeneity affecting the perfusion distribution inside the lungs. However, it is unclear if pulmonary perfusion imaging can detect substantial differences between PAH and healthy controls or assess regional changes in response to inhaled nitric oxide with oxygen. In healthy lungs, there is a vertical gradient in perfusion [5,6] including reduced lung inflation of dependent lung regions due to gravity [7]. Additionally, there is heterogeneity in perfusion within isogravitational slices that might be related to the fractal nature of the distribution of alveoli and the structure of the pulmonary vascular tree [8–10]. In addition, superimposed disease processes can lead to regional changes in lung structure or function with characteristic sizes reflected in the length-scale spectrum of perfusion heterogeneity. It is however unclear if changes in the vascular structure in PAH, such as plexiform lesions [11], increase the regional heterogeneity of perfusion associated with the specific size of affected anatomical structures. We showed that length-scale analysis of pulmonary perfusion images could detect exercise PAH at rest [12]. Other imaging studies found associations between PAH and changes in the redistribution of pulmonary perfusion in response to changes

in body position [13,14], regional pulmonary blood volume [15–17], pulmonary impedance associated with perfusion [18], and the vertical gradient in pulmonary perfusion [19]. Though early detection of PAH could improve the survival of patients [20], no pulmonary imaging parameter has been identified yet to allow a precise differentiation between PAH patients and healthy individuals,

Here, we used positron-emission tomography and high-resolution computer tomography (PET-CT) imaging for quantitatively characterize the spatial distributions of pulmonary perfusion and ventilation in patients with PAH. We compared the patterns of perfusion while breathing air and during inhalation of nitric oxide (iNO) and oxygen (O_2) (O_2+iNO) to differentiate active effects of vasoconstriction [21], anatomical structure of the vascular tree and the vertical gradient in hydrostatic pressure due to gravity. We hypothesized that differences in pulmonary perfusion images acquired at baseline and during vasodilation could identify characteristic perfusion patterns between controls and PAH subjects, even in PAH subjects deemed "non-responders" to acute vasodilation during cardiac catheterization.

METHODS

Subjects

The study was approved by the Institutional Review Board of the Massachusetts General Hospital. Informed consent was obtained from each subject before the study. We previously published an imaging study of exercise PAH [12], using the same control group as in the present study. However, there is no overlap in primary parameters and findings between both studies. Subjects enrolled with PAH at the time of recruitment, as defined by the World Health Organization Group 1 classification, were required to have a right heart catheterization (RHC) within 12 months of study entry demonstrating mPAP >25 mmHg and pulmonary capillary wedge pressure (PCWP) < 15 mm Hg.

87 Spirometry data were collected for subjects with PAH. Trends in cardiac output were non-invasively
88 recorded in all subjects using impedance cardiography (ICON, Cardiotronic, LaJolla, CA). Due to the
89 known limitations of impedance cardiography, a trend rather than an absolute change in cardiac output, was
90 monitored. For assessment of within-subject changes in perfusion and perfusion heterogeneity compared to
91 baseline and for the comparison of regional perfusion between PAH and controls, we used values of mean-
92 normalized regional perfusion obtained directly from imaging data. Pulse oximetry and heart rate were
93 continuously monitored from a fingertip pulse oximeter.

94 PAH subjects receiving vasodilators as part of their treatment were maintained on those therapies during
95 the day of study.

96 **Image Acquisition**

97 A catheter was placed in an antecubital vein for radioisotope injection. Subjects were positioned supine and
98 with arms abducted on the table of the PET-CT scanner (Biograph 64, Siemens Healthcare, Malvern PA,
99 USA). Relative lung volume was continuously measured using impedance plethysmography (SomnoStar
100 PT, SensorMedics Corp., Yorba Linda, CA, USA). After calibration of the plethysmograph, mean lung
101 volume (MLV) was determined during 30 seconds of steady tidal breathing prior to imaging. Image
102 acquisition started a 'topogram' CT scan to determine the field of view for PET and HRCT scans. In
103 preparation for an HRCT scan, the subject was asked to inhale to total lung capacity (TLC), followed by
104 slow exhalation, and to hold the breath when the impedance plethysmography signal showed that MLV was
105 reached. During the breath-hold the HRCT scan was acquired. Following this, a dynamic ^{13}NN-saline PET
106 scan was acquired starting with an equivalent breath-hold at MLV. Simultaneously with the beginning of
107 the breath-hold we injected a bolus of ^{13}NN dissolved in saline (25mL) and started the acquisition of the
108 dynamic PET scan. After 30 seconds of breath-hold, we asked the subject to resume breathing while the
109 PET scan acquisition continued. Total acquisition time of the PET scan was 6 minutes and 40 seconds.
110 During this first PET-CT imaging sequence the subject was breathing air. After it was completed, subjects

111 were administered a gas mixture (iNO, iNOMax Delivery System) of balance gas oxygen with 30 ppm
112 inhaled nitric oxide (O_2+iNO) through a one-way valve with a mouthpiece and nose clip. After at least 5
113 minutes of breathing O_2+iNO, we repeated the PET-CT imaging sequence while the subject continued to
114 breath the O_2+iNO gas mixture. Given the sample size and the desire to prevent carry over effects from the
115 inhaled nitric oxide, all subjects underwent baseline imaging followed by imaging with iNO without
116 randomization of order of imaging.

117 HRCT scans (helical mode with 64 slices per rotation, 120 kVp, and 80 mAs) were reconstructed with
118 filtered back-projection (convolution kernel B31f, 0.5 mm slice increment, voxel size: 0.7324 x 0.7324 x
119 0.5 mm^3). The PET field of view included on average 75% of the CT volume of the thorax. Dynamic PET
120 scans were reconstructed with filtered back-projection and attenuation corrections using the HRCT scan.
121 The dynamic PET scans yielded a stack of 19 images (8x5s, 3x10s, 7x30s, 60s, 2x30s), each image a 3D
122 matrix of 128x128x81 voxels (voxel size 5.3456 x 5.3456 x 2.0250 mm^3). The PET scans have a full-width
123 at half maximum (FWHM) resolution of 6 mm (Biograph 64, Siemens Healthcare, Malvern PA, USA) so
124 that the effective resolution with a contrast recovery coefficient of 80% at two times FWHM is
125 approximately 12 mm. PET images were filtered before image analysis using a moving average filter of
126 five slices (~10mm) in the axial direction and a filter with 10 mm diameter within slices, which is
127 comparable to the effective resolution of the scans.

128 **Image Analysis**

129 Image segmentation software Apollo (VIDA Diagnostics, IA, USA) was used to identify the lung region of
130 interest (ROI) in the HRCT scans. Using custom software tools written in Matlab (Mathworks, Natick,
131 MA), the lung ROIs were converted to ROI masks for PET scan analysis. Additionally, HRCT scans were
132 converted into gas fraction (F_{gas}) images using the equation:

133 F_{gas} = (tissue density – density value of the voxel) / (tissue density – density of air),

where tissue density = 0 Hounsfield units (HU) and density of gas = -1000 HU. Tissue fraction (F_{tis}) images were calculated using $F_{tis} = 1 - F_{gas}$.

Perfusion and ventilation images at baseline and after O_2+iNO were generated from ^{13}NN-saline PET scans. The analysis of dynamic PET scans of ^{13}NN kinetics following a bolus injection have been described previously [22,23]. Briefly, nitrogen gas has a very low solubility, and intravenously injected ^{13}NN, dissolved in saline, diffuses during its passage through the pulmonary capillaries rapidly out of the blood into the alveolar gas space, where it accumulates during the breath hold reaching a plateau value that is directly proportional to the local fraction of perfusion. Thus, the voxel values of a PET image of ^{13}NN activity during the plateau, divided by the mean activity within the lung represents those of a mean-normalized perfusion distribution, allowing straightforward comparisons among images taken at different conditions. After the breath hold, the subject resumes tidal breathing resulting in the washout of the ^{13}NN by ventilation with the tracer kinetics during this period yielding an estimate of specific ventilation ($s\dot{V}$) defined as: $s\dot{V}$ = alveolar ventilation ($\dot{V}_A$) / alveolar gas volume.

Assessment of regional ventilation and $\dot{V}/\dot{Q}$ ratio using ^{13}NN tracer kinetics modelling was performed as previously described [23]. Briefly, the tracer kinetics curves of each voxel were analysed to determine $s\dot{V}$, the perfusion associated with the $s\dot{V}$ kinetics, and $\dot{V}/\dot{Q}$ ratio. Four models were used for quantification of tracer washout kinetics: 1) single-exponential washout describing homogenous voxels, 2) complete gas-trapping for voxels with no change in activity during washout, 3) a double-exponential washout model describing heterogenous voxels with two compartments that have different $s\dot{V}$, and 4) a partial gas trapping model for heterogeneous voxels with one washout and one gas trapping compartment. The perfusion associated with the $s\dot{V}$ of a voxel or compartment was proportional to the initial activity of the tracer kinetics. After fitting all four models for each voxel, we used Akaike Information Criterion (AIC) (32) to select for each individual voxel the optimal model yielding $s\dot{V}$ and perfusion of the voxel or sub-voxel compartments. $\dot{V}A$ was calculated as $s\dot{V}/V$, where V = Fgas * voxel volume. For voxels with two compartments, the gas volume of each compartment was assumed to be proportional to the fraction of blood

flow in this compartment relative to the whole voxel: V_i = Fgas * voxel volume * Q_i / Q_{voxel}, were i is compartment 1 or 2, and $Q_{voxel} = Q_1 + Q_2$. Mean normalized $\dot{V}/\dot{Q}$ distributions were computed from the $\dot{V}/\dot{Q}$ ratios of the individual voxels and sub-voxel compartments using $\dot{V}_A = \dot{V}_A$ / (sum of $\dot{V}_A$ / number of voxels) and Q = Q / (sum of Q / number of voxels). $\dot{V}/\dot{Q}$ plots were constructed by binning of the typically 20,000-50,000 individual voxel and sub-voxel $\dot{V}/\dot{Q}$ values using 100 bins over the $\dot{V}/\dot{Q}$ range from 0.001 to 100. Note that the voxels with two-compartment washout kinetics were included as independent compartments [24,25]. The $\dot{V}/\dot{Q}$ dispersions of perfusion SD Q log ($\dot{V}/\dot{Q}$) and ventilation SD V log ($\dot{V}/\dot{Q}$) were calculated as the standard deviations of the perfusion-weighted and ventilation-weighted natural logarithm (Peter Wagner, personal communication, July 11, 2020) of the $\dot{V}/\dot{Q}$ distribution, respectively [26,27]. Note that other authors have used the term log SD Q, but we wanted to avoid a misinterpretation as log(SD(Q)).

Perfusion Heterogeneity and Length Scale Spectrum Analysis

Heterogeneity of perfusion was determined as the square of the coefficient of variation (CV^2 = (standard deviation/mean)^2) using a previously developed and validated method for assessment of noiseless CV^2 of PET scans based on theoretical properties of measurement errors and empirical assessment of imaging noise [28]. In short, random errors in the individual voxels of PET images, referred to as imaging noise, are superimposed to the true voxel values (signal) of the PET image and uncorrelated with the imaging signal so that the heterogeneity of an image including noise (CV^2_{Qimage}) is the sum of the variance of the true signal (perfusion) and the variance of the imaging noise $CV^2_{Qimage} = CV^2_{Qtotal} + CV^2_{noise}$ [28]. We estimated CV^2_{noise} using multiple PET images during the tracer plateau at the end of the breath-hold period and calculated the total spatial heterogeneity of ^{13}NN images of relative perfusion, excluding the imaging noise, as $CV^2_{Qtotal} = CV^2_{Qimage} - CV^2_{noise}$. In the supine position, gravitational forces typically cause a gradient in perfusion in the dorsoventral direction with higher perfusion in the dependent (dorsal) regions than in the non-dependent (ventral) regions, which can be a substantial component of CV^2_{Qtotal}. We separated the total spatial

183 heterogeneity of perfusion into components caused by systematic gradients in the vertical direction
184 (CV^2_{Qvgrad}), the axial (craniocaudal) direction (CV^2_{Qzgrad}), and the remaining, or residual heterogeneity
185 (CV^2_{Qr}). Thus, $CV^2_{Qtotal} = CV^2_{Qvgrad} + CV^2_{zgrad} + CV^2_{Qr}$. The value of CV^2_{Qr} was further split into its
186 components due to spatial variations in perfusion across the length scale spectrum [23,25]. Such a length
187 scale spectrum quantifies the components of heterogeneity originating from spatial patterns in regional
188 perfusion measured at different image resolutions.

189 For each condition, the length scale spectrum of perfusion was quantified as follows: First, the vertical and
190 the axial gradients (z direction) in perfusion (CV^2_{Qvgrad} and CV^2_{Qzgrad}) were determined. Then the gradients
191 were subtracted voxel-by-voxel from the 3D perfusion scan, and each of the resulting transverse slices of
192 the scan were low-pass filtered at 10, 30, 50, 70, 90 and 110 mm with correction for edge effects [25], CV^2
193 was calculated for each filter size, and the contribution of each length scale ranges were calculated as
194 differences between successive filter sizes, e.g. $CV^2_{Q10\text{-}30} = CV^2(10mm) - CV^2(30mm)$. Overall, small
195 length scales of a spectrum starting at 10 mm correspond to variation among volumes of approximately 1
196 mL, which corresponds to about 5 acinar units; whereas large length scales of the spatial spectrum
197 correspond to heterogeneity due to variation in structural, functional and disease processes among larger
198 regions such as segments or subsegments.

199 **Voxel Mapping and Changes in Regional Perfusion**

200 For the assessment of changes in perfusion at the voxel level, we performed elastic image registration using
201 the Advanced Normalization Tools (ANTs, free and open-source software, https://stnava.github.io/ANTs/)
202 to correct for potential tissue displacement between the two perfusion images. First, we identified the
203 transformation field that mapped the HRCT scan taken at MLV while breathing O_2+iNO to the
204 corresponding HRCT scan taken at MLV while breathing air. The same method has been successfully used
205 before to determine the regional volumetric deformation and regional lung strain during mechanical
206 ventilation [29,30]. In principle, this elastic registration method uses the density information of the HRCT

207 scans for the identification of the transformation field T(x) describing the change in tissue location from
208 one HRCT scan to the other. Image acquisition for both CT and PET scans at MLV allows for the
209 application of the transformation field T(x) to the O_2+iNO PET scan to map its voxels to the corresponding
210 voxels of the air PET scan correcting differences in tissue location. This correction is essential for an
211 assessment of changes between PET scans at the voxel level. Images representing the relative changes in
212 regional perfusion between baseline and O_2+iNO were calculated as voxel-by-voxel differences between
213 the mean-normalized perfusion at air and the mean-normalized perfusion at O_2+iNO.

214 Perfusion-height maps were generated as two-dimensional (2D) histograms of the number of voxels in
215 relation to relative perfusion and relative height from the most dorsal point of the lung mask and the most
216 ventral point. Difference maps of the perfusion-height distributions between air and O_2+iNO were
217 calculated as the difference between the perfusion-height distribution at O_2+iNO and the distribution at air.
218 Values in the difference map are visualized with a grey scale: no change equals 50% grey, decrease in
219 perfusion is lighter, and an increase is darker.

220 Mean absolute changes in regional perfusion between air and O_2+iNO were calculated at the voxel level as
221 mean absolute deviations. Contributions of imaging noise [28] to the mean deviations were removed using
222 the statistical properties of the difference image. Specifically, total variance of the difference image of
223 perfusion between air and O_2+iNO includes the sum of the variances of imaging noise in the two original
224 images. The variance of the imaging PET noise, which has a normal distribution, was determined, using a
225 previously described method for noise assessment using multiple time frames of a PET scan [28], and
226 subtracted from the total variance of the difference image. The mean absolute deviation was then calculated
227 using the relationship to the variance for a normal distribution as square root of two over pi times the
228 variance. In order to rule out that imaging noise could explain the variations in the difference image, we
229 tested in each individual study if the overall variance of the difference image was higher than the upper
230 limit of the 99.9% confidence interval of the variance from noise.

231 **Statistical Analysis**

232 Our primary outcomes of interest were the noise corrected values of total spatial heterogeneity of perfusion
233 (CV^2_{Qtotal}) and its components, including the heterogeneity generated by the vertical gradient in perfusion
234 (CV^2_{Qvgrad}) and the residual perfusion heterogeneity (CV^2_{Qr}) and its length scale components. In secondary
235 analyses, we assessed various regional perfusion and ventilation metrics. We performed two-sided T-tests
236 to evaluate whether there was a difference in means of each metric between study groups and for baseline
237 vs. O_2+iNO within study groups. Additionally, we obtained Cohen's d effect size estimates for the primary
238 parameters. All analyses were performed using R Statistical Software (v4.1.3)[31]. Effect sizes were
239 estimated using the effsize R package (v0.8.1)[32]. Statistical significance was set at $p < 0.05$. Data are
240 presented as mean (range) unless otherwise stated.

241

242 **RESULTS**

243 **Study Participants**

244 Nine subjects were studied: 5 controls, and 4 subjects with PAH (**Table 1**). Subjects were free of infections
245 or rapid progression of their disease for at least one month prior to the study and did not have any other
246 known cardiac or pulmonary disease. No subjects required oxygen therapy at the time of imaging. All
247 controls were non-smokers with subjectively normal exercise tolerance and normal pulmonary function
248 tests. All PAH subjects were initially found to have normal pulmonary function testing and normal chest
249 imaging but two of them were subsequently found to have mildly abnormal spirometry on a repeat testing
250 after imaging. PAH subjects had elevated resting mPAP (mean 43; range 33-63 mmHg) with normal PCWP
251 (mean 11; range 7-18 mmHg). Two PAH subjects were "non-responders" as demonstrated by absence of
252 significant reduction in mean pulmonary artery pressure and increased cardiac output after administration
253 of a short-acting vasodilator, one was a responder, and one did not have a standardized test. Cardiac outputs

254 were lower while breathing O_2+iNO for both groups. However, there were no significant differences in
255 cardiac output trends between groups at rest or while breathing O_2+iNO. All PAH subjects were on
256 combination therapy with a PDE5 inhibitor and endothelin receptor antagonist, and two PAH subjects were
257 also on an inhaled prostacyclin or a prostacyclin receptor agonist.

258 **Regional Perfusion Distribution: Effect of iNO and Oxygen**

259 *Total Spatial Heterogeneity in Perfusion*

260 At baseline, the total spatial heterogeneity of perfusion (CV^2_{Qtotal}) for the PAH subjects was similar to that
261 of the controls (p=0.51). However, while breathing O_2+iNO, the PAH subjects had a lower CV^2_{Qtotal} (2-
262 fold, p=0.01) compared to control counterparts (Figure 1, **Table 2**).

263 *Vertical and Axial Gradients in perfusion and the associated heterogeneity*

264 A vertical gradient in regional perfusion was observed in both groups, with higher perfusion in the
265 dependent regions (dorsal) relative to the non-dependent (ventral) regions (Figure 1, **Table 2**). At baseline
266 breathing air, the magnitude of the vertical gradient (Q_{vgrad}) and the heterogeneity generated by that gradient
267 (CV^2_{Qvgrad}) were significantly greater in the control group compared with the PAH group (p=0.04 and 0.05,
268 respectively) (**Table 2**). During O_2+iNO, these differences between groups were enhanced: CV^2_{Qvgrad} was
269 6.1-fold and Q_{vgrad} 2.9-fold, greater in the controls compared to the PAH subjects (p<0.001 and p=0.013,
270 respectively) (Figure 1, **Table 2**). Notably, during O_2+iNO, both CV^2_{Qvgrad} and Q_{vgrad} distinguished PAH
271 subjects from controls with a considerable gap between groups compared to the overlap at baseline
272 breathing air (Figure 1). Quantifying the effect size using Cohen's d, CV^2_{Qvgrad} during O_2+iNO showed the
273 largest estimate with a 95%-confidence interval not crossing zero, followed by Q_{vgrad} and CV^2_{Qtotal}: 4.30
274 (1.42, 7.17), –3.25 (–5.65, –0.84) and 2.23 (0.22, 4.25), respectively (Figure 2). In the individual subjects,
275 the average response of CV^2_{Qvgrad} to breathing O_2+iNO was an increase of 0.0272 in the controls compared
276 to a minimal decrease of -0.0017 in PAH subjects. Our study was not designed to assess differences between

277 responders and non-responders in PAH. Nevertheless, we noted that the only confirmed responder among
278 the PAH subjects showed an increase in CV^2_{Qvgrad} during O_2-iNO in the contrast to decreases in CV^2_{Qvgrad}
279 in the other three PAH subjects (Figure 1B). PAH subjects generally displayed low vertical gradients in
280 perfusion at baseline and during O_2+iNO without a significant change in the gradient (**Figures 3**). Also, the
281 differences in the vertical gradient in perfusion between groups persisted after adjusting the regional blood
282 flow by regional lung density determined from HRCT.

283 The contribution of the axial (craniocaudal) gradient in perfusion to total heterogeneity was small, and there
284 was no significant difference between the groups regardless of O_2+iNO administration (p=0.17 at baseline,
285 p=0.39 after O_2+iNO) (Figure 1C).

286 *Residual Perfusion Heterogeneity and the Length Scale Spectrum*

287 After removing the vertical and axial gradients in perfusion from the scans, PAH subjects had similar
288 residual heterogeneity (CV^2_{Qr}) when compared to controls (p=0.41) at baseline. These similarities in CV^2_{Qr}
289 remained consistent while breathing O_2+iNO. To further analyze the residual spatial heterogeneity in
290 perfusion, we assessed the variations in perfusion across the length scale spectrum. At baseline and while
291 breathing O_2+iNO, PAH subjects had similar residual heterogeneity across the spectrum of length scales of
292 10-110 mm (p>0.05 for all included length scales), when compared to control subjects (**Tables 3 & 4**).

293 *Change in Perfusion: Results of voxel mapping*

294 PAH and control subjects demonstrated significant changes in regional perfusion between air and O_2+iNO
295 at the voxel level of the two registered images (**Figures 4 & 5**) without a significant difference between
296 PAH (mean 0.19, range 0.18-0.20) and controls (mean 0.17, range 0.13-0.20). Also, the variation in regional
297 perfusion at the voxel level in each individual subject was higher than the 99.9% confidence interval
298 expected for random differences due to imaging noise, demonstrating that the perfusion distributions during
299 O_2+iNO at the voxel level were different from those while breathing air.

300 **Regional Ventilation: Effect of iNO and Oxygen**

301 Alveolar ventilation ($\dot{V}_A$) was similar between groups before and during O_2+iNO (p=0.25, p=0.49 after
302 O_2+iNO). There was no significant difference observed in the overall mean specific ventilation (s$\dot{V}$) or
303 spatial heterogeneity of $\dot{V}_A$ ($CV^2_{\dot{V}A}$) between controls and PAH subjects, reflecting a lack of parenchymal
304 lung disease (**Table 5).** Additionally, lung parenchymal density (estimated by F_{tis}) was similar between
305 control and PAH subjects.

306 **Ventilation-Perfusion Distributions: Effect of iNO and Oxygen**

307 The distributions of $\dot{V}/\dot{Q}$ ratios at baseline in PAH subjects were overall broader than in controls at baseline,
308 approaching statistical significance, consistent with moderate degrees of vascular disease-causing
309 mismatch (SD Q log ($\dot{V}/\dot{Q}$), controls 0.51 vs PAH 0.70, p=0.11). There was no difference in the $\dot{V}/\dot{Q}$
310 distribution between groups breathing O_2+iNO, in large part due to widening of the $\dot{V}/\dot{Q}$ distribution in
311 controls (SD Q log ($\dot{V}/\dot{Q}$), controls 0.65 vs PAH 0.74, p=0.58). The distributions at baseline were unimodal
312 in all subjects, except 2 PAH subjects who had bimodal distributions. $\dot{V}/\dot{Q}$ distributions during
313 administration of iNO+O_2 were unimodal in all subjects including those who had a bimodal distribution
314 prior to the intervention (**Figure 6, Table 5**).

315

316 **DISCUSSION**

317 We report a detailed analysis of regional perfusion and ventilation imaging data in PAH and control
318 subjects obtained with PET-CT, revealing unique perfusion characteristics in PAH subjects that may not
319 be reflected in routine PA pressure measurements. We found that: 1. Breathing O_2+iNO during imaging
320 resulted in significant differences in the regional distribution of perfusion between PAH subjects and
321 controls, distinguishing the subjects of the two groups. 2. CV^2_{Qvgrad} during O_2+iNO had the highest effect
322 size for PAH vs. controls. 3. All subjects in our study responded to O_2+iNO with changes in regional

323 perfusion, including the two PAH subjects who were non-responders according to vasoreactivity testing.
324 4. PAH subjects had significantly lower vertical gradients in perfusion than controls and such gradients in
325 3 of the 4 subjects were unaffected by O_2+iNO. 5. PAH subjects had residual perfusion heterogeneity
326 across the length-scale spectrum that was similar to that of controls.

327 An unexpected finding was the magnitude of the vasodilation in healthy controls during O_2+iNO leading
328 to perfusion redistributions. The significant difference in CV^2_{Qvgrad} between PAH subjects and controls
329 suggests that perfusion imaging during O_2+iNO has the potential to be as a biomarker for PAH, that could
330 lead to earlier detection and thus improve patient survival [20]. It remains unclear if the change between
331 O_2+iNO and air allows identifying responders among PAH patients. The only confirmed responder in our
332 study showed a greater response in CV^2_{Qvgrad} compared to the other PAH subjects, but it is a single case.

333 Prior studies using SPECT, MRI and PET have observed that patients with primary precapillary pulmonary
334 hypertension display a pronounced attenuation in the normal gravity-dependent distribution of lung
335 perfusion [13,14,17,19] consistent with our findings. However, these studies reported overlaps between
336 groups, reported only group means, or had not investigated the perfusion distribution during pulmonary
337 vasodilation. One study by Jones et al. [19] using adenosine demonstrated limited change in perfusion
338 redistribution and near absence of a vertical perfusion gradient in PAH even after vasodilation. Based on
339 physiologic principles, studies have hypothesized that since gravity-dependent perfusion redistribution is
340 reliant on low arterial pressures at rest and the ability to recruit and distend vessels with increased cardiac
341 output, higher pulmonary arterial pressures and loss of vascular reserves from obstructive vasculopathies
342 may inhibit vessel recruitment and distension [14,33]. Our study confirmed a lack of significant vertical
343 perfusion redistribution during exposure to O_2+iNO in those with PAH, indicating that despite measured
344 changes in regional perfusion with vasodilation, PAH subjects did not show normal vertical perfusion
345 patterns. In fact, the vertical gradient in perfusion was in some subjects nearly absent in the dependent part
346 of the lungs, as demonstrated with perfusion-height mapping (**Figure 3**), indicating that vessels at the high

347 pulmonary arterial pressures in PAH may in these subjects already be maximally recruited and distended
348 [34], and therefore are minimally affected by hydrostatic pressures.

349 An unexpected finding was that the two PAH subjects that were "non-responsive" to vasodilator in terms
350 of the definition of the guidelines for an acute response during vasoreactivity testing [3] had mean values
351 of absolute changes in voxel-by-voxel perfusion during exposure to O_2+iNO that were similar to those of
352 controls, despite having no change in their vertical gradient in perfusion. Interestingly, there is clinical
353 evidence that patients with a decrease of ≥ 30% in PVR in response to O_2+iNO benefit from vasodilator
354 therapy although they may not meet the guidelines' definition for a response during vasoreactivity testing
355 [4]. The hydrostatic pressure gradient caused by gravity would be expected to mainly effect blood vessel
356 distension, depending on the vessel compliance and tone. In this scenario, any loss of vertical gradient could
357 be thought of as a reflection of a loss of overall pulmonary vessel compliance or increase in vessel tone.
358 For instance, any mechanism narrowing the inner lumen, while the outside of the vessel is maximally
359 distended, could explain a high pulmonary vascular resistance, loss of the vertical gradient in perfusion
360 because the hydrostatic pressure gradient cannot expand the vessel, and the lack of a significant change in
361 mPAP to vasodilators. Our data suggests that some degree of vascular tone must be present since we see a
362 change in blood flow during exposure to O_2+iNO that is similar to controls. Perhaps the increase in tone
363 could be related to the smooth muscle hypertrophy that is seen in PAH [35], and the changes in regional
364 perfusion in our data could explain why some PAH patients can have symptomatic improvement with
365 vasodilators despite little change in mPAP [36].

366 Our study revealed that PAH subjects had relatively normal values of residual perfusion heterogeneity
367 across the length scale spectrum (**Tables 3 & 4**). This similarity to controls suggests that the vascular
368 disease process may not lead to increased heterogeneity among the resistances of different pathways of
369 blood flow throughout the pulmonary vascular tree. We found the lack of differences in the length scale
370 spectrum very surprising since histopathologic evaluations of the pulmonary vascular tree in patients with
371 PAH have found significant heterogeneity in the type and extent of pulmonary vascular remodelling [37–

372 39] that could have increased the heterogeneity in perfusion at some length scales linked to the anatomical
373 size of the affected sections of the vascular tree, and the length scale spectrum of perfusion heterogeneity
374 has shown differences in other studies, including exercise pulmonary arterial hypertension [12] and COPD
375 [25]. However, histopathologic samples showing structural changes cannot provide complete insights into
376 functional aspects in vivo, such as the vascular resistance along complete pathways through the vessel tree,
377 and systemic consequences of endothelial injury in pulmonary hypertension, such as alterations in the
378 coagulation system, abnormal platelet aggregation and altered production of various endothelial vasoactive
379 mediators, which may be contributing to greater uniformity in the perfusion pattern even in parts of the
380 vascular tree without histopathologic changes. Indeed, although local vascular remodelling and obstruction
381 could be expected to result in patches of low perfusion in PAH subjects, there was no evidence for
382 substantial areas of very low perfusion or significant total spatial heterogeneity of perfusion in our imaging
383 data (Figure 3 & 5). This is relevant because the ^{13}NN PET imaging technique measures the regional blood
384 flow through the alveolar capillaries, which is determined by the pressure difference between pulmonary
385 artery and pulmonary vein and the pathway resistance to blood flow. Therefore, the spatial heterogeneity
386 in perfusion includes the overall effects of vascular properties (structural and functional) as well as
387 abnormalities of the vessels along the pathways. In control subjects, O_2-iNO had no effect on the residual
388 heterogeneity of perfusion CV^2_{Qr} (Table 2), which is consistent with previous findings that hypoxic
389 pulmonary vasoconstriction had no effect on perfusion heterogeneity in healthy subjects [40].

390 The relative contribution of gravity and arterial geometry in determining pulmonary perfusion distribution
391 is still subject to debate. Hughes and West argue that gravity contributes to 24-61% of the overall variance
392 in blood flow in the human supine lung [41]. Glenny et al, on the other hand, argue that gravity accounts
393 for a minority of the variability (at most 28%) in perfusion distribution while the geometry of the vascular
394 tree, much of which is genetically predetermined, is claimed to be the primary determinate of pulmonary
395 blood flow [42]. Very few have studied the effects of vasodilation on redistribution of this vertical
396 pulmonary blood flow in healthy subjects. One prior study by Henderson et al. did not find gross

397 redistribution of pulmonary blood flow during hyperoxia in healthy subjects [43] while other studies have
398 found redistribution of blood flow [21] and increased inequality in $\dot{V}/Q$ with hyperoxia [44] and iNO [45]
399 in healthy subjects. In our study, vasodilation with O_2+iNO significantly augmented the vertical gradient
400 of perfusion and widened the $\dot{V}/\dot{Q}$ distribution in control subjects. These findings suggest that the controls
401 have baseline pulmonary vasomotor tone enhancing $\dot{V}/\dot{Q}$ matching which responds to interventions such as
402 hyperoxia and iNO.

403 The SD Q log ($\dot{V}/\dot{Q}$) values for controls in our study (0.31-0.81) are consistent with the range of values
404 previously reported in healthy adults using MIGET (0.22-0.72) [46]. Additionally, MRI-based $\dot{V}/\dot{Q}$
405 distributions are in good agreement with MIGET measurements [47]. However, MIGET using micropore
406 membrane inlet mass spectrometry (MMIMS) to measure the tracer gases resulted in narrower $\dot{V}/\dot{Q}$
407 distributions compared to MIGET using gas chromatography [48]. In contrast to MIGET, which involves
408 a smoothing function to estimate the 50 values of a $\dot{V}/\dot{Q}$ distribution from measurements of six tracer gases,
409 dynamic PET imaging of ^{13}NN tracer kinetics allows the estimations of ventilation and perfusion for up to
410 two compartments per voxel and binning of the ventilation and perfusion values to derive $\dot{V}/\dot{Q}$ distributions
411 with 100 discrete values without a smoothing function. A validation of the method using heterogenous $\dot{V}/\dot{Q}$
412 distributions has shown a good agreement between predicted and measured blood gases [49]. In PAH, $\dot{V}/\dot{Q}$
413 distributions can be substantially wider than we have found [50–53], but our results are consistent with
414 examples of narrower distributions in some PAH subjects [50,51] and the average SD Q log ($\dot{V}/\dot{Q}$) for PAH
415 in our study was slightly higher compared to controls (0.70 vs. 0.51, respectively). We cannot rule out that
416 the exclusion of regions close to the diaphragm where the tidal breathing would cause partial volume effects
417 and axial limitations in the field of view of the PET scanner had some effect on the $\dot{V}/\dot{Q}$ distribution.
418 Additionally, our PET imaging method measures relative pulmonary perfusion and the conversion to blood
419 flow, e.g., in ml/min, would require reliable cardiac output measurements during imaging, which were not
420 available in this study. Our $\dot{V}/\dot{Q}$ distributions are therefore based on mean normalized ventilation and
421 perfusion.

422 Despite our study's strengths, some important limitations should be considered. Limitations of the ^{13}NN
423 imaging technique has been discussed in detail [5,27]. Briefly, although PET scans have lower resolution
424 than CT scans, they allow assessment of functional parameters and PET resolution is more than sufficient
425 to quantify functional imaging parameters such as vertical gradients [5]. The effective spatial resolution of
426 the PET perfusion scans is approximately 12 mm, motion blurring from tidal breathing results in lower
427 spatial resolution, but our method of sub-voxel compartments can capture functional heterogeneity at this
428 level. Second, ^{13}NN tracer kinetics during the breath hold may affect the accuracy of noise-free CV^2
429 parameters of the perfusion heterogeneity, and errors in image registration causing small misalignments
430 could affect the assessment of voxel-by-voxel changes in perfusion. However, such errors only diminish
431 differences among groups and would bias our results toward the null hypothesis of statistical tests.
432 Additionally, an analysis of the reproducibility of CV^2_{Qtotal}, excluding imaging noise, in our previous
433 validation showed a standard deviation of ±8.4% in repeated imaging [28]. Third, despite notable
434 differences observed with this small cohort, future studies that include other types of patients with
435 pulmonary hypertension and larger studies with matched cohorts will be necessary to assess whether these
436 findings are more generalizable. Furthermore, additional associations may be present that we are
437 underpowered to detect in this small cohort.
438

439 **CONCLUSIONS**

440 Perfusion imaging during O_2-iNO inhalation showed a large effect size for the heterogeneity associated
441 with the vertical gradient in perfusion, $CV^2_{Qvgrad,}$ for PAH followed in magnitude by the vertical gradient
442 in perfusion. PAH subjects could be discriminated from healthy controls showing the potential of
443 CV^2_{Qvgrad} measured during O_2-iNO inhalation to be a biomarker for PAH. Further studies are needed to
444 investigate NO inhalation in clinically available imaging modalities such as dual-energy CT to translate
445 our findings into clinics.

446 **ABBREVIATIONS**

447 ^{13}NN	Isotope nitrogen-13 in a molecule bound to a stable nitrogen atom
448 2D	two-dimensional
449 3D	three-dimensional
450 6MWD	six-minute walk distance
451 AIC	Akaike Information Criterion
452 CV^2	squared coefficient of variation quantifying heterogeneity
453 CV^2_{Q10-30}	heterogeneity of perfusion at the length scale of 10 to 30 millimeter
454 CV^2_{Qr}	residual heterogeneity of perfusion
455 CV^2_{Qtotal}	total spatial heterogeneity of perfusion
456 CV^2_{Qvgrad} 457 perfusion	heterogeneity of perfusion associated with the vertical (dorso-ventral) gradient in
458 CV^2_{Qzgrad} 459 perfusion	heterogeneity of perfusion associated with the z-axail (cranio-caudal) gradient in
460 FEV_1	forced expiratory volume in first second
461 F_{gas}	gas fraction images using
462 F_{tis}	tissue fraction
463 FWHM	full-width at half maximum
464 FVC	forced vital capacity
465 HRCT	high resolution computed tomography
466 HU	Hounsfield units
467 MLV	mean lung volume
468 mPAP	mean pulmonary arterial pressure
469 MRI	magnetic resonance imaging
470 O_2+iNO	inhalation of nitric oxide (iNO) with balance gas oxygen (O_2)
471 PAH	pulmonary arterial hypertension
472 PCWP	pulmonary capillary wedge pressure

PET-CT	positron-emission tomography and high-resolution computer tomography
PVR	pulmonary vascular resistance
Q_{vgrad}	vertical (dorso-ventral) gradient in perfusion
Q_{voxel}	perfusion of a voxel
RHC	right heart catheterization
ROI	region of interest
SD Q log ($\dot{V}/\dot{Q}$)	$\dot{V}/\dot{Q}$ dispersions of perfusion
SD V log ($\dot{V}/\dot{Q}$)	$\dot{V}/\dot{Q}$ dispersions of ventilation
SPECT	single-photon emission computed tomography
$s\dot{V}$	specific ventilation
TLC	total lung capacity
$\dot{V}/\dot{Q}$	ventilation/perfusion
$\dot{V}_A$	alveolar ventilation

487 **REFERENCES**

488 1. Thenappan T, Ryan JJ, Archer SL. Evolving epidemiology of pulmonary arterial hypertension. Am J
489 Respir Crit Care Med. 2012;186:707–9.

490 2. Halliday SJ, Hemnes AR, Robbins IM, Pugh ME, Zhao DX, Piana RN, et al. Prognostic value of acute
491 vasodilator response in pulmonary arterial hypertension: beyond the "classic" responders. J Heart Lung
492 Transplant Off Publ Int Soc Heart Transplant. 2015;34:312–8.

493 3. Galiè N, Humbert M, Vachiery J-L, Gibbs S, Lang I, Torbicki A, et al. 2015 ESC/ERS Guidelines for the
494 diagnosis and treatment of pulmonary hypertension: The Joint Task Force for the Diagnosis and
495 Treatment of Pulmonary Hypertension of the European Society of Cardiology (ESC) and the European
496 Respiratory Society (ERS): Endorsed by: Association for European Paediatric and Congenital Cardiology
497 (AEPC), International Society for Heart and Lung Transplantation (ISHLT). Eur Respir J. 2015;46:903–75.

498 4. Malhotra R, Hess D, Lewis GD, Bloch KD, Waxman AB, Semigran MJ. Vasoreactivity to inhaled nitric
499 oxide with oxygen predicts long-term survival in pulmonary arterial hypertension. Pulm Circ.
500 2011;1:250–8.

501 5. Musch G, Layfield JDH, Harris RS, Melo MFV, Winkler T, Callahan RJ, et al. Topographical distribution
502 of pulmonary perfusion and ventilation, assessed by PET in supine and prone humans. J Appl Physiol.
503 2002;93:1841–51.

504 6. Prisk GK, Yamada K, Henderson AC, Arai TJ, Levin DL, Buxton RB, et al. Pulmonary perfusion in the
505 prone and supine postures in the normal human lung. J Appl Physiol Bethesda Md 1985. 2007;103:883–
506 94.

507 7. Hopkins SR, Henderson AC, Levin DL, Yamada K, Arai T, Buxton RB, et al. Vertical gradients in regional
508 lung density and perfusion in the supine human lung: the Slinky effect. J Appl Physiol Bethesda Md 1985.
509 2007;103:240–8.

510 8. Burrowes KS, Hunter PJ, Tawhai MH. Investigation of the Relative Effects of Vascular Branching
511 Structure and Gravity on Pulmonary Arterial Blood Flow Heterogeneity via an Image-based
512 Computational Model. Acad Radiol. 2005;12:1464–74.

513 9. Hlastala MP, Glenny RW. Vascular Structure Determines Pulmonary Blood Flow Distribution.
514 Physiology. American Physiological Society; 1999;14:182–6.

515 10. Nelson TR, West BJ, Goldberger AL. The fractal lung: universal and species-related scaling patterns.
516 Experientia. 1990;46:251–4.

517 11. Cool CD, Stewart JS, Werahera P, Miller GJ, Williams RL, Voelkel NF, et al. Three-dimensional
518 reconstruction of pulmonary arteries in plexiform pulmonary hypertension using cell-specific markers.
519 Am J Pathol. 1999;155:411–9.

520 12. Kohli P, Kelly VJ, Kehl EG, Rodriguez-Lopez J, Hibbert KA, Kone M, et al. Perfusion imaging
521 distinguishes exercise pulmonary arterial hypertension at rest. Am J Respir Crit Care Med.
522 2019;199:1438–41.

523 13. Horn M, Hooper W, Brach B, Ashburn W, Moser K. Postural changes in pulmonary blood flow in
524 pulmonary hypertension: a noninvasive technique using ventilation-perfusion scans. Circulation.
525 1982;66:621–6.

526 14. Lau EM, Bailey DL, Bailey EA, Torzillo PJ, Roach PJ, Schembri GP, et al. Pulmonary hypertension leads
527 to a loss of gravity dependent redistribution of regional lung perfusion: a SPECT/CT study. Heart Br Card
528 Soc. 2014;100:47–53.

529 15. Lefebvre B, Kyheng M, Giordano J, Lamblin N, de Groote P, Fertin M, et al. Dual-energy CT lung
530 perfusion characteristics in pulmonary arterial hypertension (PAH) and pulmonary veno-occlusive
531 disease and/or pulmonary capillary hemangiomatosis (PVOD/PCH): preliminary experience in 63
532 patients. Eur Radiol. 2022;

533 16. Giordano J, Khung S, Duhamel A, Hossein-Foucher C, Bellèvre D, Lamblin N, et al. Lung perfusion
534 characteristics in pulmonary arterial hypertension (PAH) and peripheral forms of chronic
535 thromboembolic pulmonary hypertension (pCTEPH): Dual-energy CT experience in 31 patients. Eur
536 Radiol. 2017;27:1631–9.

537 17. Wollmer P, Rozkovec A, Rhodes CG, Allan RM, Maseri A. Regional pulmonary blood volume in
538 patients with abnormal blood pressure or flow in the pulmonary circulation. Eur Heart J. 1984;5:924–31.

539 18. Hovnanian ALD, Costa ELV, Hoette S, Fernandes CJCS, Jardim CVP, Dias BA, et al. Electrical
540 impedance tomography in pulmonary arterial hypertension. PLOS ONE. Public Library of Science;
541 2021;16:e0248214.

542 19. Jones AT, Hansell DM, Evans TW. Quantifying pulmonary perfusion in primary pulmonary
543 hypertension using electron-beam computed tomography. Eur Respir J. 2004;23:202–7.

544 20. Lau EMT, Humbert M, Celermajer DS. Early detection of pulmonary arterial hypertension. Nat Rev
545 Cardiol. Nature Publishing Group; 2015;12:143–55.

546 21. Asadi AK, Sá RC, Kim NH, Theilmann RJ, Hopkins SR, Buxton RB, et al. Inhaled nitric oxide alters the
547 distribution of blood flow in the healthy human lung, suggesting active hypoxic pulmonary
548 vasoconstriction in normoxia. J Appl Physiol Bethesda Md 1985. 2015;118:331–43.

549 22. Melo MFV, Layfield D, Harris RS, O'Neill K, Musch G, Richter T, et al. Quantification of Regional
550 Ventilation-Perfusion Ratios with PET. J Nucl Med. 2003;44:1982–91.

551 23. Wellman TJ, Winkler T, Costa ELV, Musch G, Harris RS, Venegas JG, et al. Effect of regional lung
552 inflation on ventilation heterogeneity at different length scales during mechanical ventilation of normal
553 sheep lungs. J Appl Physiol. 2012;113:947–57.

554 24. Harris RS, Winkler T, Tgavalekos N, Musch G, Melo MFV, Schroeder T, et al. Regional pulmonary
555 perfusion, inflation, and ventilation defects in bronchoconstricted patients with asthma. Am J Respir Crit
556 Care Med. 2006;174:245–53.

557 25. Vidal Melo MF, Winkler T, Harris RS, Musch G, Greene RE, Venegas JG. Spatial Heterogeneity of Lung
558 Perfusion Assessed with 13N PET as a Vascular Biomarker in Chronic Obstructive Pulmonary Disease. J
559 Nucl Med. 2010;51:57–65.

560 26. Kelly VJ, Hibbert KA, Kohli P, Kone M, Greenblatt EE, Venegas JG, et al. Hypoxic pulmonary
561 vasoconstriction does not explain all regional perfusion redistribution in asthma. Am J Respir Crit Care
562 Med. 2017;196:834–44.

563 27. Vidal Melo MF, Layfield D, Harris RS, O'Neill K, Musch G, Richter T, et al. Quantification of regional
564 ventilation-perfusion ratios with PET. J Nucl Med. 2003;44:1982–91.

565 28. Winkler T, Melo MFV, Degani-Costa LH, Harris RS, Correia JA, Musch G, et al. Estimation of noise-free
566 variance to measure heterogeneity. PloS One. 2015;10:e0123417.

567 29. Motta-Ribeiro G, Winkler T, Hashimoto S, Vidal Melo MF. Spatial heterogeneity of lung strain and
568 aeration and regional inflammation during early lung injury assessed with PET/CT. Acad Radiol.
569 2019;26:313–25.

570 30. Motta-Ribeiro GC, Hashimoto S, Winkler T, Baron RM, Grogg K, Paula LFSC, et al. Deterioration of
571 regional lung strain and inflammation during early lung injury. Am J Respir Crit Care Med. 2018;198:891–
572 902.

573 31. R Core Team. R: A Language and Environment for Statistical Computing [Internet]. Vienna, Austria;
574 2022. Available from: https://www.R-project.org/

575 32. Torchiano M. Effsize - A Package For Efficient Effect Size Computation [Internet]. Zenodo; 2016 [cited
576 2022 May 4]. Available from: https://zenodo.org/record/1480624

577 33. West JB, Dollery CT. Distribution of blood flow and ventilation-perfusion ratio in the lung, measured
578 with radioactive CO2. J Appl Physiol. 1960;15:405–10.

579 34. Lai-Fook SJ. A continuum mechanics analysis of pulmonary vascular interdependence in isolated dog
580 lobes. J Appl Physiol. 1979;46:419–29.

581 35. Pietra GG, Capron F, Stewart S, Leone O, Humbert M, Robbins IM, et al. Pathologic assessment of
582 vasculopathies in pulmonary hypertension. J Am Coll Cardiol. 2004;43:S25–32.

583 36. Barst RJ, Gibbs JSR, Ghofrani HA, Hoeper MM, McLaughlin VV, Rubin LJ, et al. Updated evidence-
584 based treatment algorithm in pulmonary arterial hypertension. J Am Coll Cardiol. 2009;54:S78-84.

585 37. Tuder RM, Stacher E, Robinson J, Kumar R, Graham BB. Pathology of pulmonary hypertension. Clin
586 Chest Med. 2013;34:639–50.

587 38. Rol N, Timmer EM, Faes TJC, Vonk Noordegraaf A, Grünberg K, Bogaard H-J, et al. Vascular narrowing
588 in pulmonary arterial hypertension is heterogeneous: rethinking resistance. Physiol Rep. 2017;5.

589 39. Stacher E, Graham BB, Hunt JM, Gandjeva A, Groshong SD, McLaughlin VV, et al. Modern Age
590 Pathology of Pulmonary Arterial Hypertension. Am J Respir Crit Care Med. 2012;186:261–72.

591 40. Arai TJ, Henderson AC, Dubowitz DJ, Levin DL, Friedman PJ, Buxton RB, et al. Hypoxic pulmonary
592 vasoconstriction does not contribute to pulmonary blood flow heterogeneity in normoxia in normal
593 supine humans. J Appl Physiol Bethesda Md 1985. 2009;106:1057–64.

594 41. Hughes M, West JB. Point:Counterpoint: Gravity is/is not the major factor determining the
595 distribution of blood flow in the human lung. J Appl Physiol. 2008;104:1531–3.

596 42. Glenny R. Counterpoint: Gravity is not the major factor determining the distribution of blood flow in
597 the healthy human lung. J Appl Physiol. 2008;104:1533–5.

598 43. Henderson AC, Sá RC, Theilmann RJ, Buxton RB, Prisk GK, Hopkins SR. The gravitational distribution
599 of ventilation-perfusion ratio is more uniform in prone than supine posture in the normal human lung. J
600 Appl Physiol Bethesda Md 1985. 2013;115:313–24.

601 44. Barberà JA, Roger N, Roca J, Rodriguez-Roisin R, Rovira I, Higenbottam TW. Worsening of pulmonary
602 gas exchange with nitric oxide inhalation in chronic obstructive pulmonary disease. The Lancet.
603 1996;347:436–40.

604 45. Katayama Y, Higenbottam TW, Diaz de Atauri MJ, Cremona G, Akamine S, Barbera JA, et al. Inhaled
605 nitric oxide and arterial oxygen tension in patients with chronic obstructive pulmonary disease and
606 severe pulmonary hypertension. Thorax. 1997;52:120–4.

607 46. Cardús J, Burgos F, Diaz O, Roca J, Barberá JA, Marrades RM, et al. Increase in Pulmonary
608 Ventilation–Perfusion Inequality with Age in Healthy Individuals. Am J Respir Crit Care Med.
609 1997;156:648–53.

610 47. Sá RC, Henderson AC, Simonson T, Arai TJ, Wagner H, Theilmann RJ, et al. Measurement of the
611 distribution of ventilation-perfusion ratios in the human lung with proton MRI: comparison with the
612 multiple inert-gas elimination technique. J Appl Physiol Bethesda Md 1985. 2017;123:136–46.

613 48. Kretzschmar M, Schilling T, Vogt A, Rothen HU, Borges JB, Hachenberg T, et al. Multiple inert gas
614 elimination technique by micropore membrane inlet mass spectrometry—a comparison with reference
615 gas chromatography. J Appl Physiol. 2013;115:1107–18.

616 49. Vidal Melo MF, Harris RS, Layfield JDH, Venegas JG. Topographic basis of bimodal ventilation-
617 perfusion distributions during bronchoconstriction in sheep. Am J Respir Crit Care Med. 2005;171:714–
618 21.

619 50. Bratel T, Lagerstrand L, Brodin L-A, Nowak J, Randmaa I. Ventilation-perfusion relationships in
620 pulmonary arterial hypertension: effect of intravenous and inhaled prostacyclin treatment. Respir
621 Physiol Neurobiol. 2007;158:59–69.

622 51. Dantzker DR, Bower JS. Mechanisms of gas exchange abnormality in patients with chronic
623 obliterative pulmonary vascular disease. J Clin Invest. 1979;64:1050–5.

624 52. Mélot C, Naeije R, Mols P, Vandenbossche JL, Denolin H. Effects of nifedipine on
625 ventilation/perfusion matching in primary pulmonary hypertension. Chest. 1983;83:203–7.

626 53. Voswinckel R, Reichenberger F, Gall H, Schmehl T, Gessler T, Schermuly RT, et al. Metered dose
627 inhaler delivery of treprostinil for the treatment of pulmonary hypertension. Pulm Pharmacol Ther.
628 2009;22:50–6.

629

630 **FIGURE LEGENDS**

631 **Figure 1: Perfusion heterogeneity profiling distinguished PAH subjects and control subjects.** The
632 total spatial heterogeneity of perfusion (CV^2_{Qtotal})[28] (**A**) is comprised of the heterogeneity of the vertical
633 (dorsoventral) gradient in perfusion (CV^2_{Qvgrad}) (**B**), the heterogeneity of the craniocaudal (z-axis) gradient
634 in perfusion (CV^2_{Qzgrad}) (**C**), and the heterogeneity of the residual (or remaining) perfusion (CV^2_{Qr}) (**D**).
635 PAH subjects demonstrated very low CV^2_{Qvgrad} due to attenuated vertical gradients in perfusion (Q_{vgrad})
636 (**E**) that were not responsive to O_2+iNO, distinguishing this cohort from their control counterparts. Note
637 that imaging noise is excluded from all CV^2 parameters.

638 **Figure 2: Cohen's d effect size estimates and 95% confidence intervals of the primary parameters.**
639 The effect sizes for PAH vs. control were substantially larger for O_2+iNO compared to baseline. CV^2_{Qvgrad}
640 had the most significant effect size and a 95% confidence interval not crossing zero, followed by Q_{vgrad} and
641 CV^2_{Qtotal}. The relatively large effect sizes for O_2+iNO vs. baseline in the control group are indicators of the
642 magnitude of the response.

643

644 **Figure 3: Perfusion-height maps for PAH subjects and controls.** The greatest perfusion heterogeneity,
645 including the largest range of perfusion values at any given height, was present in PAH subjects, followed
646 by controls. The vertical gradient in perfusion (represented by the slope of the black-and-white dashed line)
647 increased in magnitude in controls but not PAH subjects breathing O_2+iNO. In contrast to controls, several
648 PAH subjects had no vertical gradient in perfusion in the lower or dependent part of the lung (dorsal in the
649 supine position), as if the hydrostatic pressure, which increases towards the dependent regions, had no effect
650 on perfusion. Surprisingly, there was no substantial fraction of voxels with very low or zero perfusion in
651 any PAH subject, suggesting there was no severe or complete obstruction of blood vessels. The only
652 confirmed responder of the PAH group is shown in the second row.

Figure 4: Difference maps of the perfusion-height distribution visualizing the changes in mean normalized perfusion vs. height in response to the administration of O_2+iNO in PAH subjects and controls. Note that all subjects had regional responses to breathing O2+iNO, including PAH subjects who had no discernible change in mean pulmonary arterial pressures with vasodilator challenge during cardiac catheterization. In controls, the changes in perfusion show a substantial spatial heterogeneity with an overall trend towards an increased vertical gradient during O2+iNO and more uniform perfusion in the dependent (dorsal) regions (see also Fig. 2). In contrast, there are substantial changes in regional perfusion in PAH but not associated with a shift in the vertical gradient except for the confirmed responder among the PAH subjects shown in the second row. All panels use the same scale greyscale for the magnitude of differences.

Figure 5: 3D renderings and animations of perfusion distributions. (A) Representative 3D renderings of the mean-normalized distribution of perfusion for PAH and healthy control subjects at baseline and after O_2+iNO (animated in Videos V1 (https://doi.org/10.6084/m9.figshare.12442589) and V2 (https://doi.org/10.6084/m9.figshare.12442784)) showing the effects of the administration of O_2+iNO based on PET-CT imaging in supine position. The patchy areas of high perfusion illustrate the size and location of regional variations behind the representations in perfusion-height maps (Fig. 2). **(B)** 3D renderings of the regional changes in perfusion corresponding to the perfusion distributions in panel A(animated in Videos V3 (https://doi.org/10.6084/m9.figshare.12442787) and V4 (https://doi.org/10.6084/m9.figshare.12442790)). The web-like structure of perfusion increases (yellow) and decreases (blue) instead of gradual changes in perfusion among different regions illustrates the spatial variations behind the difference maps of the perfusion-height distribution (Fig. 3). The relatively small sizes suggest the involvement of smaller anatomical structures together with larger anatomical structures linked to the average changes in larger regions. In all 3D renderings, the orientation of the lungs is shown by a small mannequin. Color scales are fully transparent either for average perfusion (A, V1, and V2) or zero change (B, V3, and V4), opaqueness increases with the deviation from these values, and differences in color between PAH and controls are differences in magnitude. Rotating 3D renderings with periodic switching between air and O2+iNO show the location and changes in high and low perfusion areas. This provides a spatial perception of their location and their magnitude lacking in the still images – video download provides the highest resolution and allows playback in loop mode.

682 **Figure 6: $\dot{V}/\dot{Q}$ distributions in PAH subjects and controls.** The distributions of $\dot{V}/\dot{Q}$ ratios at baseline
683 in PAH subjects were overall broader than in controls at baseline, approaching statistical significance,
684 consistent with moderate degrees of vascular disease, causing a mismatch. There was no difference in the
685 $\dot{V}/\dot{Q}$ distribution among groups while breathing O_2+iNO, in large part due to the widening of the $\dot{V}/\dot{Q}$
686 distribution in controls. $\dot{V}/\dot{Q}$ distributions while breathing O_2+iNO were unimodal in all subjects,
687 including those with a bimodal distribution prior to the intervention.

688 **TABLES**

689 **Table 1 Baseline characteristics**

Parameter	Control N=5	PAH N=4	p-value
Age (years)	41.2 (22-60)	47.3 (22-64)	0.64
Gender, Female	1	3	0.14
Race, White	5	3	0.39
Height (inches)	67.3 (63-71.5)	67.2 (66-68.5)	0.91
Weight (pounds)	189.6 (160-296.7)	170.5 (124-264)	0.67
Years of symptoms	NA	8.4 (7-10)	
FEV1 (%predicted)	NA	82.9 (66-95)	
FVC (% predicted)	NA	85.6 (64-110)	
FEV1/FVC	NA	80 (63-86)	
mPAP, rest (mmHg)	NA	41.6 (33-63)	
PVR, rest (dyn·s/cm^5)	NA	442 (322-548)	
PCWP, rest (mmHg)	NA	10 (7-16)	
6MWD (feet)	NA	1519.8 (1253-2198)	

Continuous variables are represented as mean (min-max). Categorical variables are represented as counts.

Definitions of abbreviations: PAH = primary pulmonary arterial hypertension; FEV_1 = forced expiratory volume in first second; FVC= forced vital capacity; mPAP = mean pulmonary arterial pressure; PVR = pulmonary vascular resistance; PCWP = pulmonary capillary wedge pressure; 6MWD = six-minute walk distance.

690 **Table 2 Vertical gradient and heterogeneity in perfusion**

Parameter	Control		PAH	
	Baseline	**O_2+iNO**	**Baseline**	**O_2+iNO**
Q_{vgrad} (10^{-2} cm^{-1})	-5.46 (-3.32, -7.01)*†	-7.37 (-6.43, -8.66)*‡	-3.13 (-2.33, -4.78)†	-2.51 (-0.039, -0.431) ‡
CV^2_{Qtotal}	0.09 (0.06, 0.16)	0.12 (0.08, 0.16)‡	0.08 (0.07, 0.11)	0.06 (0.04, 0.1)‡
CV^2_{Qvgrad}	0.04 (0.02, 0.08)†	0.08 (0.055, 0.10)‡	0.01 (0.0, 0.03)†	0.01 (0.0002, 0.02)‡
CV^2_{Qr}	0.04 (0.02, 0.07)	0.04 (0.02, 0.06)	0.05 (0.04, 0.06)	0.03 (0.02, 0.04)

Continuous variables are represented as mean (min, max).

Definitions of abbreviations: PAH = primary pulmonary arterial hypertension; Q_{vgrad} = vertical gradient in regional perfusion (slope); CV^2_{Qtotal} = squared coefficient of variation in perfusion quantifying total spatial heterogeneity of perfusion (noise corrected); CV^2_{Qvgrad} = squared coefficient of variation in perfusion quantifying heterogeneity generated by the dorsal-ventral gradient in perfusion; CV^2_{Qr} = squared coefficient of variation in perfusion quantifying heterogeneity of the residual perfusion.

* significant difference between measures at baseline and during administration of O_2+iNO within a group

† significant difference between PAH subjects and controls at baseline

‡ significant difference between PAH subjects and controls while breathing O_2+iNO

691 **Table 3 Perfusion Distributions at all Length Scales at Baseline**

Parameter	Controls	PAH	p-value
CV^2_{Q10-30} ($x10^{-3}$)	13.0 (6.82, 29.77)	19.7 (17.17, 22.25)	0.33
CV^2_{Q30-50} ($x10^{-3}$)	7.77 (4.06, 16.70)	10.0 (8.05, 11.70)	0.68
CV^2_{Q50-70} ($x10^{-3}$)	4.46 (2.59, 8.15)	5.61 (4.48, 6.83)	0.45
CV^2_{Q70-90} ($x10^{-3}$)	2.52 (1.69, 3.57)	3.31 (2.54, 4.67)	0.20
$CV^2_{Q90-110}$ ($x10^{-3}$)	1.48 (0.96, 2.10)	1.91 (1.41, 3.22)	0.33
$CV^2_{Q>110}$ ($x10^{-3}$)	5.28 (1.19, 16.83)	5.81 (0.80, 21.04)	0.80

692 Definition of abbreviations: $CV^2_{Q(lengthscale)}$ = squared coefficient of variation in perfusion quantifying

693 spatial heterogeneity in regional perfusion in the denoted length scale range (mm)

694 **Table 4 Perfusion Distributions at all Length Scales at During O_2+iNO**

Parameter	Controls	PAH	p-value
CV^2_{Q10-30} ($x10^{-3}$)	14.4 (6.65, 24.32)	13.4 (8.24, 17.43)	0.62
CV^2_{Q30-50} ($x10^{-3}$)	8.43 (4.68, 12.80)	7.16 (4.66, 9.59)	0.46
CV^2_{Q50-70} ($x10^{-3}$)	4.62 (2.44, 6.07)	4.04 (2.50, 6.48)	0.68
CV^2_{Q70-90} ($x10^{-3}$)	2.61 (1.29, 3.26)	2.32 (1.48, 3.91)	0.72
$CV^2_{Q90-110}$ ($x10^{-3}$)	1.51 (0.75, 1.98)	1.40 (1.04, 2.06)	0.70
$CV^2_{Q>110}$ ($x10^{-3}$)	9.56 (5.46, 20.68)	4.66 (4.05, 5.23)	0.10

695 Definition of abbreviations: CV2Q(length scale) = squared coefficient of variation in perfusion

696 quantifying spatial heterogeneity in regional perfusion in the denoted length scale range (mm)

697 **Table 5 Regional F_{tis} and Ventilation parameters at baseline and during O_2+iNO**

Parameter	Control		PAH	
	Baseline	**O_2+iNO**	**Baseline**	**O_2+iNO**
F_{tis}	0.35 (0.31, 0.43)	0.39 (0.33, 0.49)	0.34 (0.27, 0.37)	0.37 (0.33, 0.41)
Volume (ml)	2107 (1521, 2646)	1940 (1421, 2347)	2223(1676, 3209)	2147 (1282, 2997)
Mean $s\dot{V}$ ($10^{-3}s^{-1}$)	2.69 (1.49, 4.13)	2.92 (2.21, 3.51)	4.68 (1.82, 9.72)	3.33 (2.00, 5.91)
$\dot{V}_A$ (ml/min)	5.56 (3.73, 8.53)	5.55 (4.26, 6.72)	9.36 (4.22, 16.30)	6.31 (3.85, 7.84)
$CV^2_{\dot{V}A}$	0.19 (0.07, 0.33)	0.18 (0.12, 0.24)	0.32 (0.07, 0.54)	0.28 (0.09, 0.37)

Continuous variables are represented as mean (min, max).

Definitions of abbreviations: PAH = primary pulmonary arterial hypertension; F_{tis} = tissue fraction; Volume = gas volume; V_A = alveolar ventilation; $s\dot{V}$ = specific ventilation ($\dot{V}_A$ /alveolar volume); $CV^2_{\dot{V}A}$ = squared coefficient of variation quantifying heterogeneity in alveolar ventilation.

698

699

700 **DECLARATIONS**

701 **Ethics approval and consent to participate**

702 The study was approved by the Institutional Review Board of the Massachusetts General Hospital. Informed
703 consent was obtained from each subject before the study.

704 **Consent for publication**

705 Not applicable.

706 **Competing interests**

707 The authors declare that they have no competing interests. For full disclosure, ASW has been consulting
708 for United Therapeutics in the past on topics unrelated to this study, and RC has or had consultant, research,
709 or speaker relationships with United Therapeutics, Janssen, Bayer, Gossamer, Altavant, Third Pole, and
710 Aria CV.

711 **Availability of data and materials**

712 The datasets used and/or analysed during the current study are available from the corresponding author on
713 reasonable request.

714 **Funding**

715 Support for this research was provided by an unrestricted grant from United Therapeutics. The sponsor was
716 not involved in the study design, analysis, or reporting of study findings.

717 **Author information**

718 Tilo Winkler and Puja Kohli contributed equally as joint first authors.

719 **Affiliations**

720 The following is the list of author affiliations at the time the study was conducted. Changes are listed under
721 acknowledgements.

722 ***Department of Anesthesia, Critical Care and Pain Medicine, Massachusetts General Hospital and***
723 ***Harvard Medical School, Boston, Massachusetts, USA***

724 Tilo Winkler PhD, Jose G. Venegas PhD

725 ***Division of Pulmonary and Critical Care Medicine, Department of Medicine, Massachusetts General***
726 ***Hospital and Harvard Medical School, Boston, Massachusetts, USA***

727 Puja Kohli MD MMSc, Vanessa J Kelly PhD, Ekaterina G. Kehl MD, Alison S. Witkin, MD, Josanna
728 Rodriguez-Lopez MD, Kathryn A. Hibbert MD, Mamary Kone MD MPH, Richard Channick MD, R. Scott
729 Harris MD

730 ***Division of Pulmonary and Critical Care Medicine, Department of Medicine, Brigham and Women's***
731 ***Hospital and Harvard Medical School, Boston, Massachusetts, USA***

732 David M. Systrom MD, Aaron B. Waxman MD

733 **Contributions**

734 Study design: MK, EGK, RC, RSH; data acquisition: TW, PK, VJK, EGK, JRL, KAH, MK, DMS, JGV,
735 RC, RSH; data analysis: TW, PK, VJK, RSH; data interpretation: TW, PK, RSH; manuscript drafting and
736 editing: PK, TW, VJK, RSH; all authors read and approved the final manuscript.

737 **Corresponding author**

Tilo Winkler, PhD – email: twinkler@mgh.harvard.edu

Massachusetts General Hospital

Dept of Anesthesia, Critical Care and Pain Medicine

55 Fruit Street, Boston, MA 02114

USA

Acknowledgements

The authors thank the staff from the Massachusetts General Hospital Departments of Nuclear Medicine and Nuclear Pharmacy for their assistance with this project, including Steve Weise, Michael Cournoyer, John Correia, Eugene Lee, Peter Rice, Melissa Bruen, Erin Beloin, Kevin Vernon and Daniel Yokell. In addition, the authors extend kind thanks to Julian Fischer and Gabriel C. Motta-Ribeiro for their contributions to the process of image registration, Rebecca Harris for her contributions to mask creation, Benno F. Rodemann for his contribution to media creation and to Pradeep Natarajan MD (Massachusetts General Hospital, Division of Cardiology) for helpful discussions and feedback on this work. The present address of Richard Channick is David Geffen School of Medicine at UCLA, Los Angeles, California, USA, and the address of Ekaterina G. Kehl is Division of Pulmonary and Critical Care Medicine, Mount Auburn Hospital, and Harvard Medical School, Boston, Massachusetts, USA.

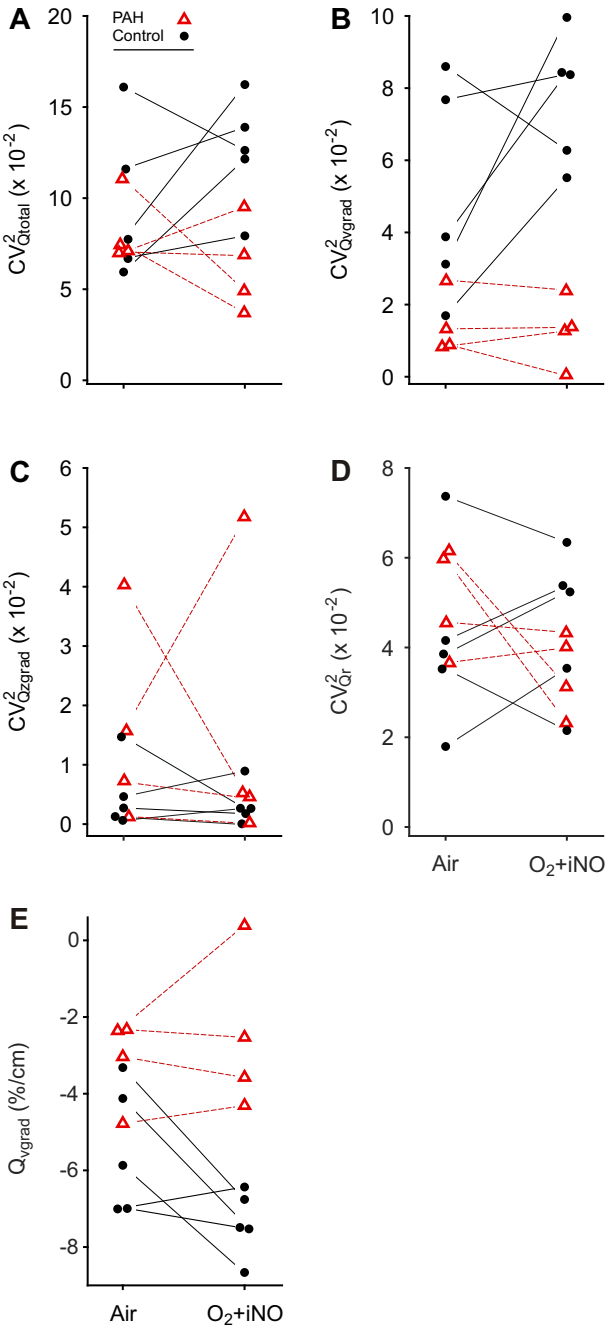
A
PAH
Control
CV^2_{Qtotal} (x 10^{-2})
B
CV^2_{Qvgrad} (x 10^{-2})
C
CV^2_{Qzgrad} (x 10^{-2})
D
CV^2_{Qr} (x 10^{-2})
Air
O_2+iNO
E
Q_{vgrad} (%/cm)
Air
O_2+iNO

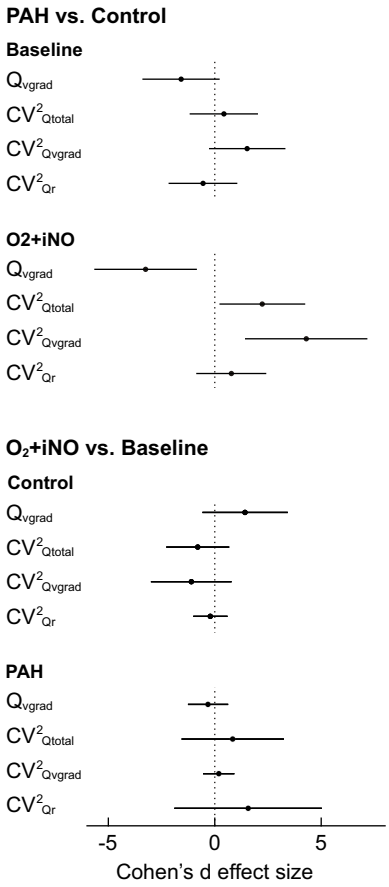
PAH vs. Control
Baseline
Qvgrad
CV2Qtotal
CV2Qvgrad
CV2Qr
O2+iNO
Qvgrad
CV2Qtotal
CV2Qvgrad
CV2Qr
O2+iNO vs. Baseline
Control
Qvgrad
CV2Qtotal
CV2Qvgrad
CV2Qr
PAH
Qvgrad
CV2Qtotal
CV2Qvgrad
CV2Qr
-5
0
5
Cohen's d effect size

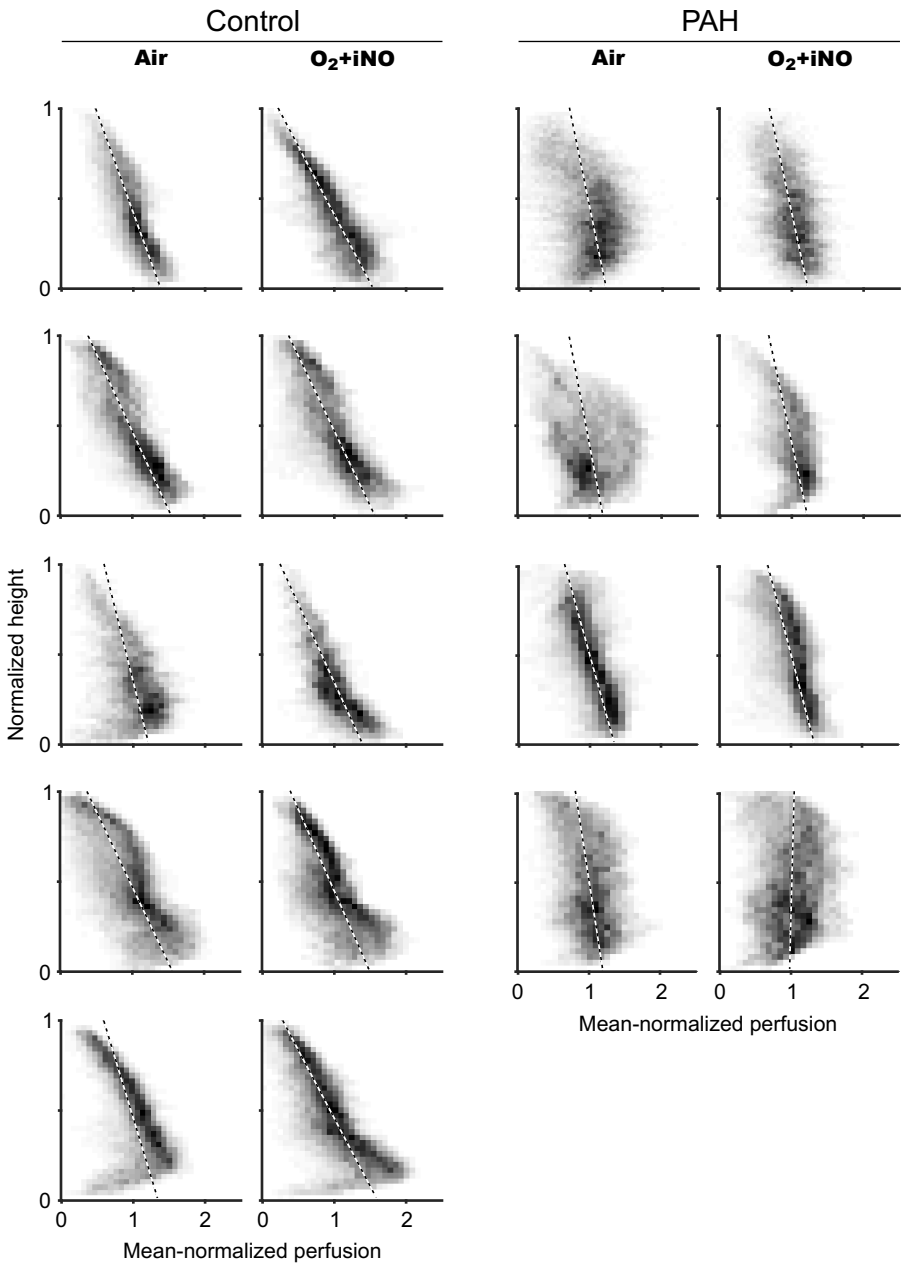
Control
PAH
Air
O_2+iNO
Air
O_2+iNO
Normalized height
1
0
0
1
2
Mean-normalized perfusion

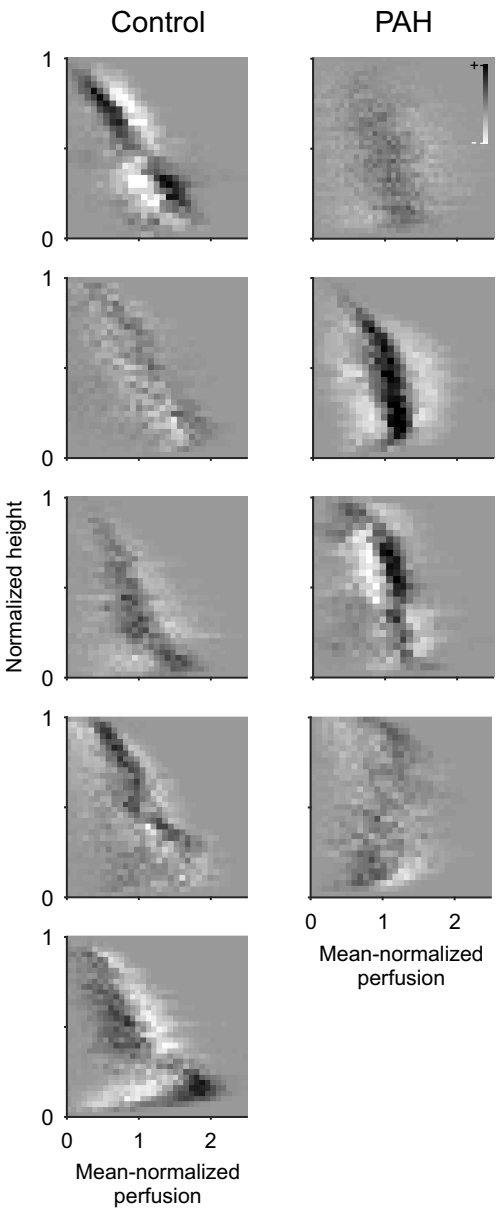
Control
PAH
Normalized height
1
0
0
1
2
Mean-normalized perfusion
Mean-normalized perfusion

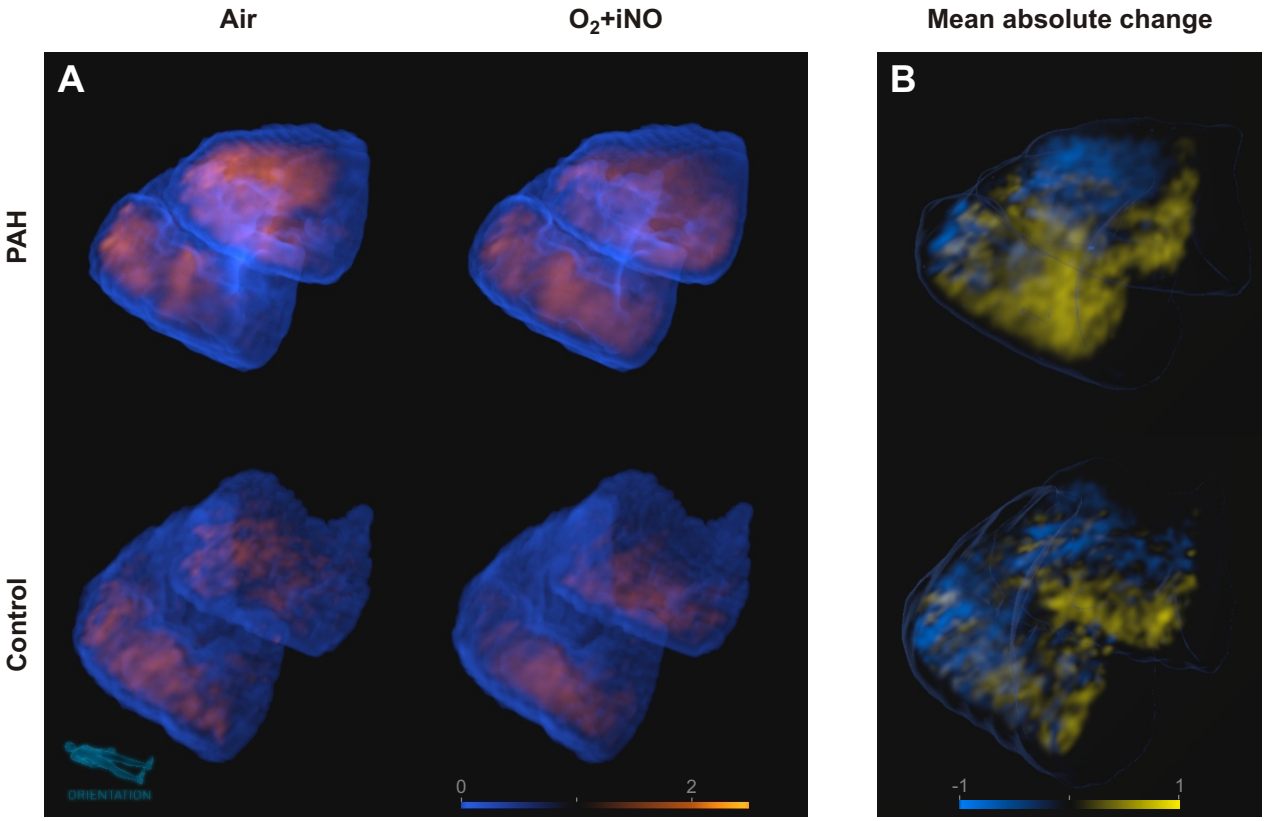
Air
O2+iNO
Mean absolute change
A
B
PAH
Control
ORIENTATION
0
2
-1
1

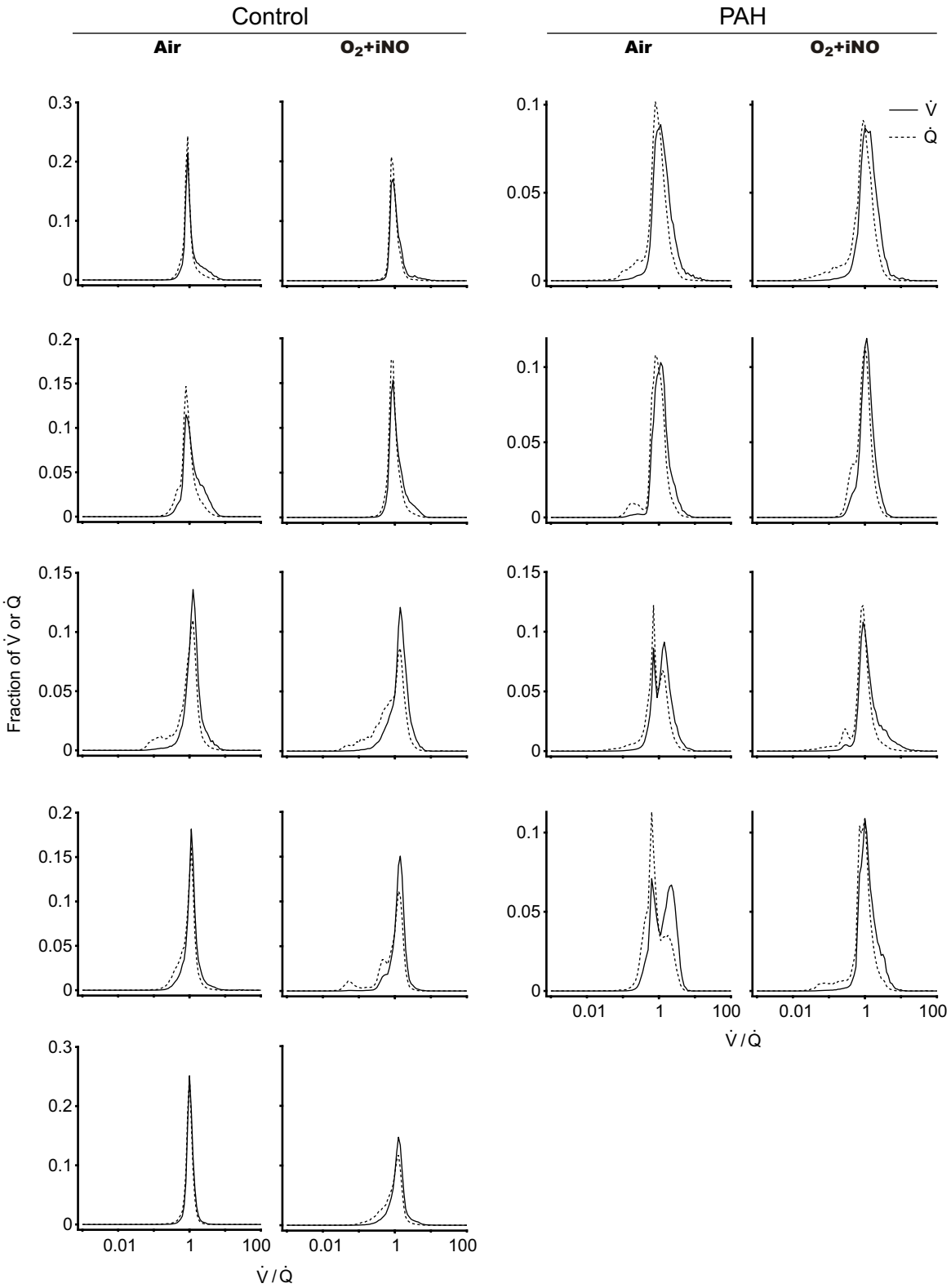
Control
PAH
Air
O2+iNO
Air
O2+iNO
V̇
Q̇
Fraction of V̇ or Q̇
V̇ / Q̇
0.01
1
100